Accepted to Phys. Fluids 10.1063/5.0184410

Experimental study on the flow-induced vibrations of a circular cylinder with a rear flexibly-hinged splitter plate

J. C. Muñoz-Hervás,[1,2] M. Lorite-Díez,[3,4] J. Ruiz-Rus,[1,2] and J. I. Jiménez-González[1,2,a)]

[1)] *Departamento de Ingeniería Mecánica y Minera, Universidad de Jaén, 23071 Jaén, Spain*

[2)] *Andalusian Institute for Earth System Research, Universities of Granada, Jaén and Córdoba, 23071 Jaén, Spain.*

[3)] *Andalusian Institute for Earth System Research, Universities of Granada, Jaén and Córdoba, 18006 Granada, Spain.*

[4)] *Departamento de Mecánica de Estructuras e Ingeniería Hidráulica, Universidad de Granada, 18001 Granada, Spain*

(Dated: 20 December 2023)

The flow around a circular cylinder is a canonical configuration that may be encountered in many engineering applications, as for instance, civil engineering, architecture, or marine structures. In particular, when bluff bodies are slender and feature low mass-damping characteristics, they may undergo flow-induced vibrations which may result in severe structural fatigue and damage.

Here, we present an experimental study on the effect of flexibly-hinged splitter plates in the flow-induced vibrations (FIV) of a flexibly-mounted circular cylinder (of diameter D) subject to an uniform cross-flow of velocity u_∞. The dynamic response and forcing of the low mass-damping system is characterized for plates of different lengths L_p and different values of the torsional stiffness of the hinge k_p.

Reductions of the dynamic response of more than 90% can be generally reached at the upper branch, especially when a plate of length $l^* = L_p/D = 2$ with intermediate degree of torsional stiffness is attached, which is shown to represent the best solution as it mitigates the oscillations of the system (cylinder and plate) for the whole range investigated of reduced velocity $U^* = u_\infty/f_n D = [3.9, 9.8]$, where f_n is the natural frequency of oscillation. In general, the hinged plates are able to attenuate the vortex-induced vibration system response by increasing shedding frequency, until the ratio $f^* = f/f_n > 1$ is reached. At high values of U^*, a general transition to galloping-like dynamics, characterized by $f^* < 1$, occurs. The tested hinged plates modify the transition between regimes, which is associated to shifts in the phase difference between the forcing and response, combining features of the dynamics of both flexible and static rigid plates already reported in the literature.

The use of hinged plates has been proven to provide with a significant attenuation of the system response and its associated drag, a feature that can be considered of practical relevance in many engineering applications. In addition, the key aspects for designing these elements as the torsional stiffness and plate length have been analysed here.

I. INTRODUCTION

The flow around a circular cylinder in low mass-damping systems may produce flow-induced vibrations (FIV)[1,2]. That configuration is a simple representation of many engineering applications where a structure is submerged in water or air flows.

In the case of the circular cylinder, this vibrating dynamics may be induced by vortex shedding that leads to vortex-induced vibrations (VIV). That particular response is char-

[a)] jignacio@ujaen.es

Accepted to Phys. Fluids 10.1063/5.0184410

acterized by a self-limited oscillation, guided by the synchronization between the vortex shedding in the wake of the cylinder and the natural frequency of the system[3,4].

The periodic vibration of slender parts may result in structural fatigue damage and, consequently, control of FIV has attracted traditionally the scientific interest, which has given rise to a large amount of work devoted to FIV characterization and control[3,5–7]. Within the literature on the subject of mitigating VIV, various passive techniques have been suggested. These techniques encompass solutions such as helical strakes, control rods, wire meshes, fairings, and splitter plates, among others[5,8].

While most of these systems are capable of suppressing efficiently the FIV, configurations such as fairing or rear plates, which renders the structure elongated and asymmetric with respect to relative misaligned flow conditions, may result into enhanced vibrations of increasing amplitude with the flow velocity[9,10]. In particular, this dynamics is characteristic of unstable galloping-like responses, which are generally linked to a synchronized excitation with the cross-flow force and a slower dynamics due to added mass effects[11].

Rigid splitter plates, attached to the rear of the cylinder, have been traditionally proposed as efficient control devices to reduce flow excitation and decrease the drag acting on static cylinders[8]. As shown by Apelt, West, and Szewczyk [12], long plates may help reducing interaction between shear layers from both sides of the cylinder, affecting the shedding process and the aspect ratio of the separated recirculating region.

For freely oscillating cylinders, the use of rear plates can be however counterproductive when the relative stiffness is low. This occurs for large values of the reduced velocity, which is defined as $U^* = u_\infty/f_n D$, where u_∞ is the incident flow velocity, while f_n and D are the natural oscillation frequency of the cylinder and its diameter, respectively. Thus, as shown by Assi and Bearman [13], short plates with length $l^* \leq D$ can already trigger galloping-like responses of systems with low mass ratio $m^* = m_s/m_f \simeq 2$ (with m_s and m_f being respectively the structure and fluid mass). In that work, flow visualizations indicated that due to the shear layer reattachment onto the splitter plate, the excitation is fostered. The influence of the shedding on the galloping-like response was already highlighted by Stappenbelt [14], who also found that cylinder mounting long plates with $l \geq 4D$ do not show enhanced vibrations.

Similar results have been recently retrieved numerically and experimentally by Zeng *et al.* [15], for different lengths of splitter plate and a cylinder-plate system with large mass ratio of $m^* = 50$. The threshold for the stabilization of the galloping response is, however, Reynolds dependent, as shown therein and in Sahu *et al.* [16].

On the contrary, when flexible plates are considered, the system presents the ability to adapt its relative position with respect to the incident flow, what may help decreasing the amplitude response over a wide range of small and moderate values of the reduced velocity, as shown by Cui and Feng [17] and Cui, Feng, and Hu [18]. In particular, the adaptive dynamics of the flexible plates prevents the interaction between the upper and lower shear layers, reducing the excitation. However, if secondary modes of vibrations of plates are activated, what may occurs at large reduced velocities, the cylinder's response can be amplified and galloping-like responses are triggered, as reported e.g. experimentally and numerically by Liang *et al.* [19] and Sahu, Furquan, and Mittal [20].

The previous results demonstrate that the introduction of additional degrees of freedom (dof) to the vibrating system may help attenuating the FIV response in comparison to rigid plates.

In that sense, alternative configurations of lower mechanical order, such as multi-body solutions, can be also adapted. For instance, the additional degrees of freedom can be achieved by allowing rotary oscillations of the splitter plate or the cylinder-plate system around the pivoting axis[21,22], or by mounting the plate with a hinge at the rear attachment point[23]. The own dynamics and rotation of the rear plates alter considerably the shedding process, and may reduce the amplitude of the oscillating lift acting on the body, as reported by Gu *et al.* [24] for the static cylinder.

The use of free-to-rotate plates as a control device of VIV was experimentally explored by Assi, Bearman, and Kitney [25] and Assi, Bearman, and Tognarelli [26]. In particular, Assi,

Accepted to Phys. Fluids 10.1063/5.0184410

Bearman, and Kitney [25] showed that the rotary plate may reduce the FIV response when compared to the plain cylinder, as long as enough torsional resistance is set for the pivoting point.

Besides, the use of flexibly-hinged plates, like those investigated by Shukla, Govardhan, and Arakeri [23] for the static cylinder, has not been yet analyzed in FIV applications of cylinders. Thus, to the best of the authors' knowledge, the only study dealing with such configuration is the numerical work by Wu, Shu, and Zhao [27], which examine the problem for a fixed laminar Reynolds number of $Re = 150$, and using a plate length of $0.5D$. This arrangement is shown to reduce the VIV oscillations for low values of U^*, but displays unstable galloping-like responses at large values of U^*, in a similar manner to the rigid plate of same length. The enhanced vibrations are shown to be associated to the reattachment of the shear layers at the plate tip. However, this behavior cannot be generalized to higher Reynolds numbers and longer plates. Thus, considering that such an arrangement has attracted less attention of researchers, the control effect of hinged plates, designed with a flexible torsional joint, on low mass-damping systems, in this case a circular cylinder, subjected to flow induced vibrations at moderate Reynolds numbers, is not clear.

In that regard, we study experimentally the effect of flexibly-hinged plates of different lengths and different torsional stiffness on the dynamic response of an elastically-mounted circular cylinder subject to turbulent cross-flow. The work aims to analyze the behavior of the system and compare it to those of flexible and rigid plates. The paper is organized as follows: the problem description and experimental details are introduced in Sect. II. Next, Sect. III is devoted to analyze the results on the dynamic response of the different cylinder-plate systems while Sect. IV shows flow visualizations of the near wake. The analysis of the force coefficients is presented in Sect. V. Finally, the main conclusions are drawn in Sect. VI.

II. EXPERIMENTAL DETAILS

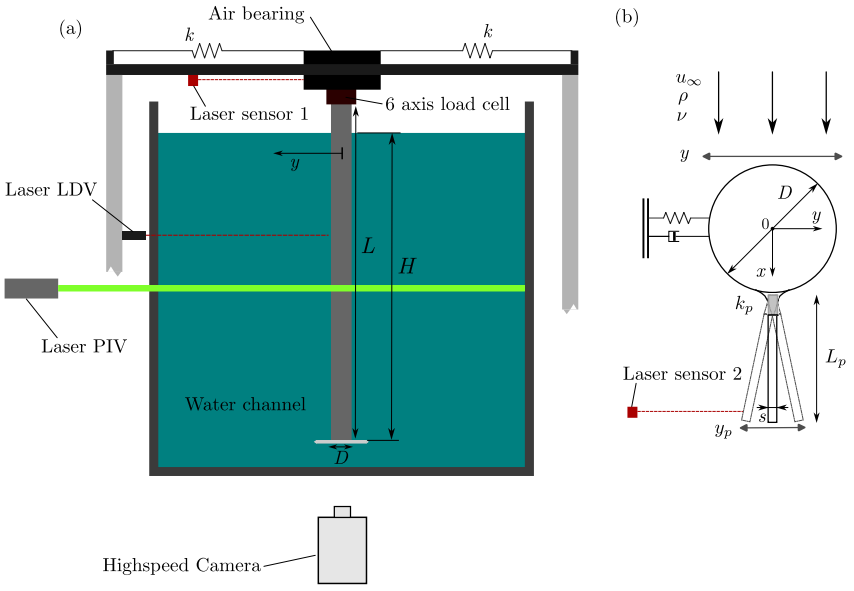

FIG. 1. (a) Experimental Set-up and (b) sketch of the problem.

Experiments were conducted in the Free Surface Water Channel at Universidad de Jaén (UJA). The water channel has a cross-section of 0.4×0.5 m^2 and it is able to deliver over 0.6 m/s. The velocity profile in the working section is characterised by a very low velocity variability, with a maximum deviation of 2%.

Accepted to Phys. Fluids 10.1063/5.0184410

Figure 1 displays schematic representations of the experimental set-up of two-degrees of freedom. The first degree of freedom consists in an elastically-mounted rigid acrylic tube that acts as a circular cylinder of diameter $D = 32$ mm, which can move in the transverse direction of the flow. The second consists in a rigid plate of length L_p and thickness $s = 3$ mm ($s/D = 0.094$), which is flexibly hinged at the rear end of the main cylinder, and covers the whole cylinder length. The models were submerged 0.36 m yielding a length-to-diameter aspect ratio of $L/D = 11.25$. The assemble had an end-plate attached to his bottom end that prevented three-dimensional effects. Two springs were connected to the cylinder model providing restoring forces to the system, that hung from an air bearing rig that allowed the cylindrical model to oscillate in the cross-flow, y. Two PLA 3D printed parts acted as a support for the trailing cylinder, fixing it to the rig.

Additionally, the rigid acrylic plates were hinged at the rear of the cylinder by means of a flexible torsional joint modelled of silicone rubber, allowing the plates to perform angular oscillations, with a tip displacement y_p (see Fig. 1b). Thus, the cylinder-plate arrangement behaves as a a two-degrees-of-freedom system.

The structural parameters characterizing the problem are the mass ratio, m^*, and the structural damping, ξ. Considering the cylinder-plate assemble, the former is defined as

$$m^* = \frac{m_s}{\frac{1}{4}\rho_f \pi L D^2 + \rho L L_p s}, \tag{1}$$

where $m_s = m_c + m_p + m_a$ is the total mass of the system, given by the addition of that of cylinder m_c, plate m_p and a small additional mass of value m_a placed on the rig and used when needed to keep the value of $m^* = 11$ constant for all arrangements considered, i.e. isolated cylinder and cylinder-plates. Free-decay tests in air were performed to obtain the structural damping of the isolated cylinder and cylinder-plate systems, observing very small differences around the averaged value of $\xi = 0.0018$. Thus, considering the previously given value of m^*, the averaged combined mass-damping parameter was found to be $m^*\xi = 0.02$.

Besides, additional free decay tests in air of the rotary oscillations of the plates, while keeping static the main cylinder, allowed determination of their natural frequency, f_p. Subsequently, torsional stiffness of each flexible joint k_p can be estimated from

$$f_p = \frac{1}{2\pi}\sqrt{\frac{k_p}{J_p}}, \tag{2}$$

where J_p is the polar moment of inertia of the plates, and considering the plates rotation as that of an 1 degree-of-freedom angular oscillator. The damping rate was also obtained from such decay tests of rotary damped oscillations, obtaining an averaged value of $\xi_p = 0.03$.

The Reynolds number based on the cylinder model diameter $Re = u_\infty D/\nu$, where u_∞ and ν are respectively the free-stream velocity and the water kinematic viscosity, ranged from approximately 3800 to 15200. The ratio between the free stream velocity in the channel and the average velocity of the cylinder (based on its natural frequency in water f_n) is defined as the reduced velocity $U^* = u_\infty/f_n D$, being the range covered in the experiments $U^* = [3.6, 9.8]$. The wake frequencies are made non-dimensional using the Strouhal number defined as $St = f_w D/u_\infty$, where f_w is the experimentally measured shedding frequency in the wake of the fixed circular cylinder.

Seven different control configurations have been tested, comprising three different plate lengths, $l^* = L_p/D = [1, 2, 3]$ or (l_1^*, l_2^*, l_3^*), and four different torsional stiffness of the hinged-like junction, $k_p = [0.034, 0.096, 0.598, \infty]$ N $\cdot$ m/rad or $(k_{p1}, k_{p2}, k_{p3}, k_{p4})$, aside from the isolated plain cylinder. In particular, the stiffness of the flexible joint was varied using silicone rubbers of different shore hardness, allowing to study the following values of k_p for the parametric analysis. The $k_p \to \infty$ case represents the rigid limit, obtained by rigidly fixing and gluing the plate to the cylinder. Note that this variable can be expressed in dimensionless form as $k_p^* = 2\pi k_p/\rho u_\infty^2 D^3$, which represents the ratio of joint torsional stiffness to a hydrodynamic stiffness, or as a reduced velocity $U_p^* = u_\infty/f_p D$, but these magnitudes vary with flow velocity.

Accepted to Phys. Fluids 10.1063/5.0184410

The motion of the cylinder and the flexibly-hinged splitter plate is characterized by using respective non-intrusive precise optical laser displacement sensors Leuze ODSL-8/VC66-200-S12 (with a measurement range from 20 to 200 mm, with a resolution lower than 0.2 mm), placed in the experimental set-up as shown in Fig. 1. The first sensor captures the motion of the cylinder along the air bearing rig, $y^* = y/D$, while the second one measures the tip displacement of the tested plate, $y_p^* = y_p/D$, which is computed here relative to the cylinder motion, $y^* = y/D$.

Besides, the flow forces acting on the cylinder along the cross-flow, f_y, and in-line (drag), f_x, directions were measured using a multi-axial precise load cell SRI-M3703A (with 50 N range in x, y directions, with $< 0.5\%$ non-linearity and hysteresis and $< 2\%$ cross-talk effects). Thus, dimensionless force coefficients were obtained as

$$c_i = \frac{\mathrm{f}_i}{0.5\rho u_\infty^2 DH}, \tag{3}$$

being c_x and c_y the drag and cross-flow or lift coefficients respectively, and H the submerged height of the cylinder. According to the load cell accuracy, these coefficients have an associated uncertainty of ± 0.001.

All the previous measurements were performed with an acquisition frequency of $f_s = 1000$ Hz sampling during at least 180 s, ensuring enough temporal resolution to capture the system dynamics properly. Considering that the minimum measured oscillation frequency in water was 1.3 Hz, at least 200 oscillation cycles were recorded for each test. Besides, to ensure repeatability of results, 3 different runs were performed for each different configuration, observing very low dispersion ($< 1\%$ of the averaged value) in the obtained results.

Moreover, flow characterization was performed by means of PIV measurements to complement the understanding of the mechanisms behind the system dynamic response. In order to obtain the streamwise, u, and the transversal, v, velocity components, an horizontal laser sheet was produced with a 1.5 W Diode-Pumped Solid-State (DPSS) green laser (Novanta LAQ-GEM-532-1500) equipped with cylindrical and spherical lenses. The laser sheet was placed at mid height of the cylinder to illuminate the near wake region behind the moving arrangement (see Fig. 1a). The flow was seeded with 20 μm neutrally-buoyant polyamide particles and recorded with a Photron Fastcam SA 1.1, with a resolution 1024 px $\times$ 1024 px up to 5400 fps, equipped with a 60 mm F/2.8 objective and a 532 nm filter. The recorded 1024 px $\times$ 1024 px images were captured synchronized with the laser displacement sensors at 125 and 250 fps, depending on the flow velocity, to cover at least 20 shedding cycles. Also, the exposure time was modified for the different conditions to acquire images of focused seeding particles. The recorded images were preproccesed making use of a specifically developed algorithm. Firstly, the solid moving parts were detected, obtaining a moving mask for the following PIV processing. Then, an improvement of the particle's intensity was achieved through a contrast enhancement process, which involved the subtraction of a background reference image and the normalization of the image brightness[28]. In order to obtain the velocity vectors through time-resolved particle image velocimetry (TR-PIV), we have used the Matlab toolbox PIVlab[29]. The velocity vectors were obtained using interrogation windows of 48 px $\times$ 48 px with a 50% overlapping, which resulted in a spatial resolution of 3 mm. Our field of view covers a region of view 119 mm $\times$ 119 mm with a scaling factor of 8 px/mm, which is enough to characterize the main flow features in the near wake. The temporal velocity in the wake at ($x^* = 3$, $y^* = 0.5$) was also obtained using a Laser Doppler Velocimeter system (model MSE mini LDV), obtaining very similar results to PIV ones.

Finally, note that, in the following, any time-dependent variable will be denoted using lower case letters, e.g. b, while its temporal averaging will be expressed by means of capital letters, $B = \overline{b}$, unless otherwise stated. Note that, to evaluate the amplitude of the time-dependent variable as b, we will apply the Hilbert transform to obtain the instantaneous amplitude (envelope), $\hat{b}$, being $\hat{B}$ its average.

Accepted to Phys. Fluids 10.1063/5.0184410

III. DYNAMIC RESPONSE

In this section, we present the dynamic response of the different control plate arrangements investigated, as a function of the reduced velocity U^* (and Reynolds number Re), which are compared to that corresponding to the plain cylinder. Two different parametric studies are shown, namely: (a) the effect of varying control plate's length $l^* = L_p/D = [1, 2, 3]$ for a given torsional stiffness of the flexible joint $k_p = k_{p2} = 0.096$ N·m/rad; and (b) the effect of varying torsional stiffness of the flexible joint $k_p = [0.034, 0.096, 0.598, \rightarrow \infty)$ N·m/rad, for a given length of control plate $l^* = 2$. The FIV dynamic response is characterized by the oscillation averaged amplitude $\hat{A}$ and main frequency f, which are non-dimensionalized using respectively the main cylinder diameter, D, and the natural frequency of the cylinder system, f_n, to give $\hat{A}^* = \hat{A}/D$ and $f^* = f/f_n$.

A. Plain cylinder

The complete curves of amplitude and frequency responses with respect to reduced velocity U^*, are depicted in Fig. 2(a1 and a2) for the plain cylinder. These curves are obtained by processing the temporal evolution of the cylinder y^*-displacement for each reduced velocity. The processing involves determining the averaged oscillation amplitude $\hat{A}^*$ using the Hilbert transform and identifying the main frequency f^* of the vibration by means of analysis of Power Spectral Density function PSD(f^*) (see Fig. 2b1 and b2 for the selected values of $U^* = 5.3$ and 9.0.)

Thus, the uncontrolled case shows the classical amplitude and frequency curves for VIV of flexibly mounted cylinders in water, consisting of initial, upper and lower branches, being largest amplitudes reached within the upper branch ($\hat{A}^* \simeq 0.75$). The oscillation frequency, identified in Fig. 2(a2) with help of contours of Power Spectral Density PSD(f^*), grows linearly as U^* is increased along the initial branch, following the Strouhal law ($St \simeq 0.18$, identified by LDV measurements), to reach a plateau within the upper branch, $5 < U^* < 6$, that defines the *lock-in* or synchronization range with $f^* \simeq 1$, where the amplitude is largest. From here on, the frequency rate f^* remains nearly constant along the lower branch, where the amplitude response decreases. These differences between upper and lower branches are easily observable in Fig. 2(b1 and b2), where individual time-sequences (note that $t^* = tu_\infty/D$) and corresponding PSD are plotted for two illustrative values of U^*.

B. Effect of the plates length

Let us now focus on the controlled cylinder-plate system, whose dynamic response is considerably different to the baseline case, as it will be next discussed. We first depict in Fig. 3(a1 and a2), results when plate's length is varied for a given constant value of the torsional stiffness. Thus, the amplitudes $\hat{A}^*$ and main frequency ratio f^* are shown as a function of reduced velocity U^*, for the different lengths $l^* = [1, 2, 3]$ of the hinged plate. The response of the isolated cylinder is also shown as reference case. In general, the amplitudes are markedly reduced in the upper and lower branches when the plates are mounted, and little trace of response branches remains. However, differences are encountered when the plate's length changes. In particular, the use of a plate of $l^* = 2$ attenuates the dynamic response of the system for the whole range of U^* investigated. Reductions in the amplitude of nearly 95% are reported for the upper branch, with its maximum at $U^* = 6.6$. However, for plates with $l^* = 1$ and $l^* = 3$, the picture differs and, in spite of providing general reductions of the vibrating response, a linear increase of $\hat{A}^*$ is observed for the lower branch, so that amplified vibrations can be expected beyond the range of U^* studied here. This may be an indication of galloping-like behaviour, where oscillations are not self-limited, as reported in classical problems of FIV of cylinders with static splitter

Accepted to Phys. Fluids 10.1063/5.0184410

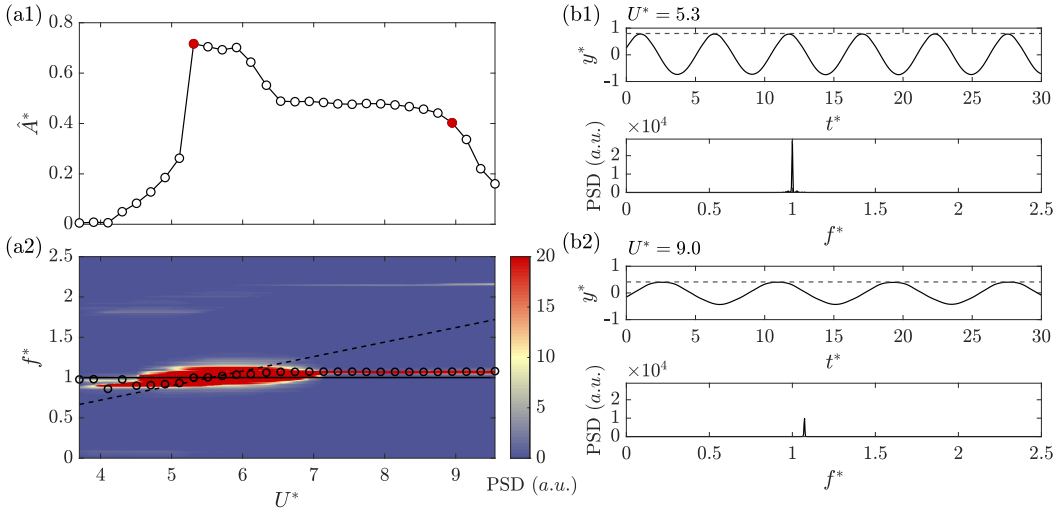

FIG. 2. Dynamic response for the plain cylinder case: (a1) amplitude response $\hat{A}^*$ and (a2) frequency response f^* versus reduced velocity U^*; (b) temporal amplitude response $y^*(t^*)$ (where $t^* = tu_\infty/D$) with its mean amplitude (dashed line) and corresponding Power Spectral Density function, PSD(f^*) for the selected values of reduced velocity $U^* = 5.3$ (b1) and 9.0 (b2) (red points a1). In (a2) dominant frequencies are identified using circles representing maximum amplitudes in the contours of the PSD(f^*), while dashed line represents the Strouhal law given by $f^* = St \cdot U^*$, ($St \simeq 0.18$) and $f^* = 1$ is included by a solid line.

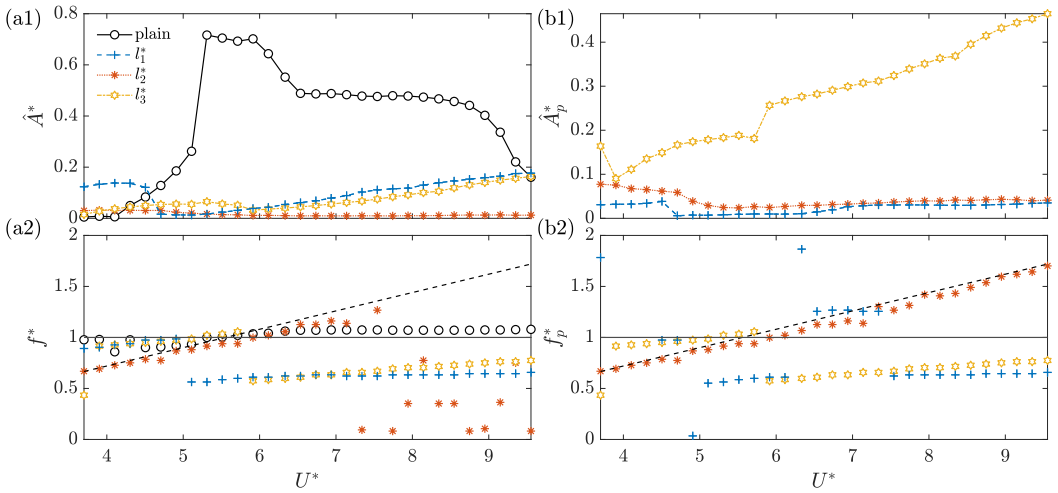

FIG. 3. (a1) Amplitude and (a2) frequency responses of the controlled system of cylinder with plates of different lengths $l^* = [1, 2, 3]$ for an intermediate value of joint stiffness $k_p = 0.096$ N · m/rad, and (b1) corresponding tip amplitude and (b2) frequency responses of the relative displacement of mounted plates with respect to the cylinder.

plates (see e.g. Stappenbelt [14]). Interestingly, the shortest plate shows also an intensified response at low U^*.

The frequency response is also modified with the addition of plates, as shown in Fig. 3(a2). In particular, $l^* = 1$ and 3 show similar responses characterized by the initial vibration at frequencies slightly lying above the Strouhal line $f^* > St \cdot U^*$ and close to unity. This is especially clear for the shortest plate, where the vibration frequency is locked near the natural frequency, what may explain the amplified amplitude response at low U^*. As U^* increases above 5, the oscillation frequency displays a lock-in range with $f^* < 1$ for both

Accepted to Phys. Fluids 10.1063/5.0184410

configurations, which is a typical feature of galloping-like responses.

For $l^* = 2$, the frequency response follows the Strouhal law initially, while the oscillations are discernible in the amplitude response (Fig. 3a1). However, after $U^* \simeq 6.5$ no coherent pattern is observed as the vibration is inhibited.

These types of response are somehow similar to previously reported results in the literature for FIV of cylinders with rear rigid splitter plates. For instance, Assi and Bearman [13] studied the effect of placing a free-to-rotate splitter plate of $l^* = 1$, observing a similar increase of the amplitude response at low U^*, governed with frequencies close $f^* = 1$ and above the Strouhal law; while galloping is reported at large reduced velocity. The galloping type response reported here for higher values of U^* is however noticeably weaker in terms of amplitude, what might stem from the slight adaptation of plate to flow, as it presents mild oscillations on account of the finite stiffness of the torsional joint. Note that Assi, Bearman, and Kitney [25] reported mitigated responses when a certain degree of torsional resistance is set to the rotation point of the plate. Besides, the decrease of the frequency response for $U^* > 5$ may be related to a higher added mass produced by the addition of large plates that displace larger amount of fluid[30]; we shall discuss this issue later when forces are presented. In fact, this effect seems to be exclusively related to added mass, as the mass ratio m^* has been kept constant for all experiments (using additional mass when required) and is not affected by the addition of longer plates.

To further elucidate the nature of the tested system oscillations, we present in Fig. 3(b1 and b2) the relative tip transverse amplitude and frequency responses of the mounted plates around the pivoting point at the rear of the cylinder. Thus, it is observed that the relative amplitude $\hat{A}_p^*$ grows in general with l^*, with the shorter plates showing weak relative oscillations, which are stronger at lower values of the reduced velocity U^* (i.e. where the relative stiffness of the hinge is larger). However for $l^* = 3$ a seemingly unstable response characterized by an increasing amplitude A_p^* with growing U^* is displayed. This dynamic of the plate may promote the stronger excitation of the cylinder depicted in Fig. 3(a1). Besides, as observed in Fig. 3(b2), the $l^* = 2$ plate mainly oscillates following the vortex shedding frequency given by the Strouhal law (depicted using a dashed line), while the shorter and longer plates follow this law initially, to subsequently start vibrating at a rate $f_p^* < 1$ at large U^*, which is also shown to guide the cylinder-plate system vibrations for such reduced velocities. The frequency jumps observed in Fig. 3 (b1 and especially b2) are caused by the quasi-periodic nature of the system response for the l_1^* and, especially l_3^* plates. At certain reduced velocities, the $f^* \simeq 1$ and $f^* \simeq 0.5$ frequency peaks have similar amplitude that provokes the observed frequency jumps. However, neither bistable nor hysteretic behaviours have been observed at the whole range of tested U^*.

These trends and magnitudes are somewhat similar to those reported by Cui, Feng, and Hu [18] for flexible foils installed at the rear of a flexibly-mounted cylinder. This is however different from what was reported by Shukla, Govardhan, and Arakeri [23] for hinged plates behind static cylinder, whereby shorter plates display larger amplitudes, highlighting again the specific dynamic nature of the combined two-degrees-of-freedom system of cylinder and plate.

The coupled dynamics is further analyzed in terms of the flapping process of plates of different lengths and its phase with respect to the cylinder's vibration. The flapping of plates is illustrated, for selected reduced velocity at upper ($U^* = 5.3$) and lower ($U^* = 9.0$) branches, with help of Fig. 4(a), where the range of the cylinder's motion and the plate's relative angular displacement are shown with help of selected snapshots. The time history of the linear displacement of cylinder y^* and plate's tip y_p^*, along with their corresponding PSD and phase portraits (y_p^*, y^*) are depicted respectively in Fig. 4(b), (c) and (d). The flapping sketches in (a) and time histories in (b) show the progressive increase of the vibrating amplitude with growing length l^*, for both selected values of U^*, as already illustrated in Fig. 3. Besides, different coupled dynamics between cylinder and plate is observed in terms of frequency and phase for different lengths. For instance, the vibration of the shortest plate $l^* = 1$ is in general weak (Fig. 4b1,b4), since the plate is shorter than the vortex formation length for these kind of flows, as it will be shown in Sect. IV. Its vibration occurs

Accepted to Phys. Fluids 10.1063/5.0184410

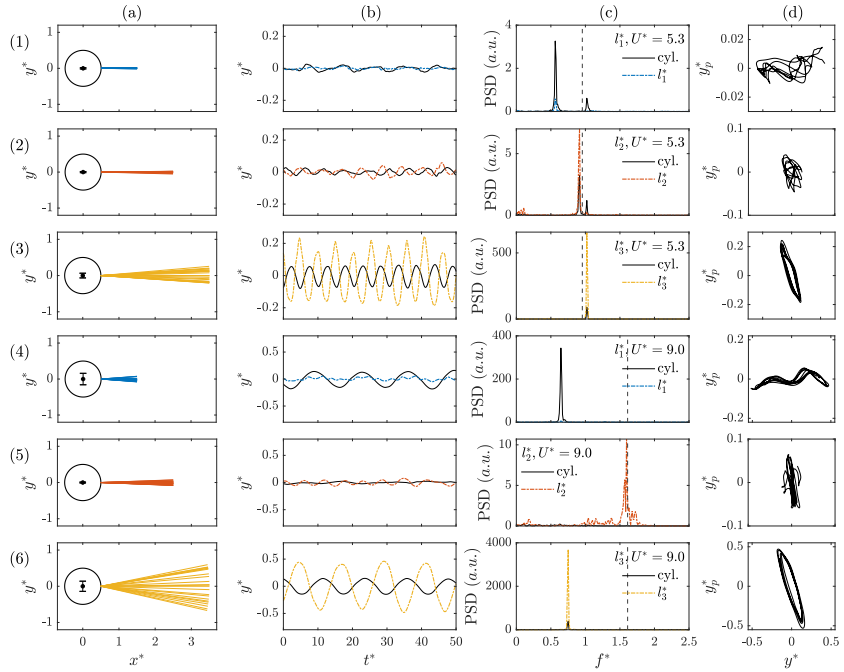

FIG. 4. (a) Sketches of the flapping process of the hinged plates and cylinder motion, (b) time histories (note that $t^* = tu_\infty/D$) of the flapping displacement of the hinged plate tip y_p^* (coloured solid lines) and the cylinder displacement y^* (black solid lines), (c) power spectral density of the plate and cylinder oscillations; and (d) corresponding phase portraits $y_p^* - y^*$, for $l^* = 1$, 2 and 3. The selected cases and reduced velocity are $U^* = 5.3$ (1-3) and $U^* = 9.0$ (4-6), for plate's length $l^* = 1$ (1,4), 2 (2,5) and 3 (3,6). Note that in (d) x-axis and y-axis marks are identical for each phase portrait. The Strouhal value for each corresponding reduced velocity has been included in (c) by black dashed lines.

approximately at the same frequency and seemingly in phase with the oscillation of the cylinder, as displayed in Fig. 4(c1,c4). More precisely, at $U^* = 5.3$, the dynamics of the system is characterized by two frequencies in the PSD (Fig. 4c1), whose peaks correspond to a galloping-like frequency $f^* < 1$ and the natural frequency of the system $f^* = 1$. The concurrence of multiple frequencies and some lag between attenuated signals lead to the irregular phase portrait displayed in Fig. 4(d1). However, for $U^* = 9.0$, the cylinder vibration is periodic and enhanced, which is presumably due to an added mass effect, as inferred from the dominant frequency in the PSD is $f^* < 1$.

Thus, the phase portrait in Fig. 4(d4) displays a sort of elongated quasi-periodic orbits with some meandering, due to the concomitant periodic oscillations of the cylinder and the mild quasi-periodic dynamics of the plate.

For $l^* = 2$, the plate vibration is slightly amplified with respect to the previous case, but the general dynamics is considerably attenuated. The plate is shown to vibrate unfairly (Fig. 4b2, b5) following the vortex shedding (Fig.3a2, b2), and therefore the frequency rate is $f^* < 1$ for $U^* = 5.3$, whereas for $U^* = 9.0$ the dominant frequency is $f^* > 1$, as displayed in Fig. 4(c2, c5). As discussed earlier, the VIV of the cylinder is nearly suppressed for both values of the reduced velocity. The lack of coherence in the phase lag between oscillations of the cylinder and plate (see Fig. 4b2, b5) may contribute, together with the globally attenuated vibration amplitude, to the definition of compact and seemingly irregular phase portraits (Fig. 4d2, d5).

Finally, the dynamics of the $l^* = 3$ system is clearly more periodic. As observed, the flapping features a periodic nature, and there is a good coupling between cylinder and plate vibrations, as illustrated in the PSD and phase portraits, which show closed orbits,

Accepted to Phys. Fluids 10.1063/5.0184410

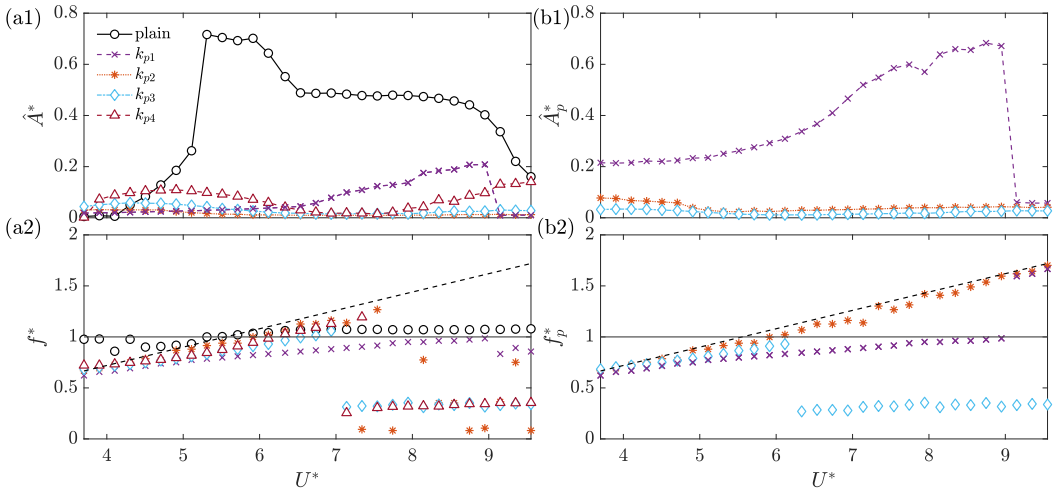

FIG. 5. (a1) Amplitude and (a2) frequency responses of the controlled system of cylinder with plates of different joint stiffness $k_p = [k_{p1}, k_{p2}, k_{p3}, k_{p4}] = [0.034, 0.096, 0.598, \infty]$ N · m/rad for length $l^* = 2$, and corresponding (b1) amplitude and (b2) frequency responses of the relative displacement of mounted plates with respect to the cylinder.

associated to nearly periodic dynamics. The slight meandering of the orbits is linked to the modulation of the plate's amplitude identified in Fig. 4(b3, b6). The vibration of the plate and cylinder follows the shedding frequency ($f^* = 1$) at $U^* = 5.3$ (Fig. 4c3), but it is guided by a lower frequency, $f^* < 1$, at $U^* = 9.0$, as occurred for the shortest plate. In spite of the amplified oscillations of the longest plate, the excitation of the cylinder is not as efficient, which may be due to the fact that the plate and cylinder vibrates out of phase, as depicted in the time series of Fig. 4(b3, b6).

These results show that there seems to be an highly effective length of $l^* = 2$, given a value of $k_p = 0.096$ N·m/rad, for which the oscillations are suppressed within the range of reduced velocity herein analyzed. However, the role of the torsional stiffness of the joint still needs to be addressed, to check whether this magnitude affects the plate adaptation to the flow changes, and therefore to the vortex-induced vibrations of the cylinder.

C. Effect of the stiffness of the torsional joint

Figure 5 displays the effect of increasing torsional stiffness $k_p = [k_{p1}, k_{p2}, k_{p3}, k_{p4}] = [0.034, 0.096, 0.598, \infty]$ N·m/rad on the dynamic response of plates with $l^* = 2$. Note that the case of k_{p2} has been already discussed in the previous section since it corresponded to the case $l^* = 2$, and will be used as reference now. As illustrated in Fig. 5(a1), the amplitude response is in general weak, regardless of the value of k_p, although its value modify the nature of response. Thus, it seems that there is an optimal interval for intermediate values of the torsional stiffness, as the most flexible k_{p1} and rigid k_{p4} cases display less attenuated amplitudes.

The most flexible joint k_{p1} displays efficient suppression of the oscillations along the initial ($U^* \leq 5.1$) and upper ($5.1 < U^* < 6.1$) branches, although an increasing amplitude is observed for the reduced velocity range $6.1 < U^* < 9$, coincident with the interval of the original lower branch. At $U^* = 9$ the amplitude decays suddenly, to achieve complete suppression of the oscillations.

As observed in Fig. 5(a2), the frequency response follows approximately a linear trend, which lies however below that of the shedding frequency of the plain cylinder $St \cdot U^*$. This trend is maintained until $U^* = 9$, where $f^* \simeq 1$. From here on, the oscillations are attenuated and the frequency decreases. This coupled dynamics of the system is seemingly

Accepted to Phys. Fluids 10.1063/5.0184410

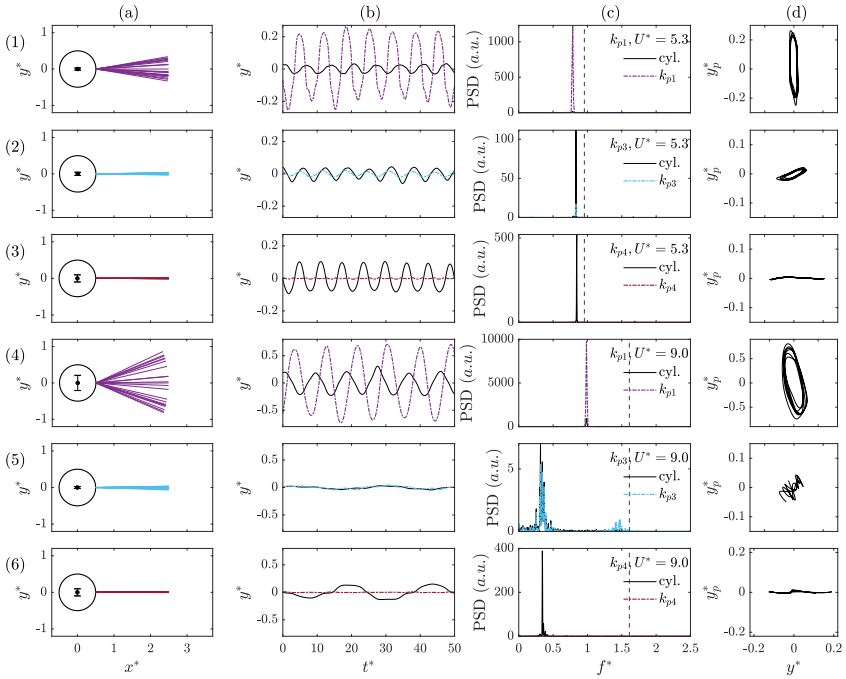

FIG. 6. (a) Sketches of the flapping process of the hinged plates and the cylinder motion, (b) time histories (note that $t^* = tu_\infty/D$) of the flapping displacement of the hinged plate tip y_p^* (coloured solid lines) and the cylinder displacement y^* (black solid lines), (c) power spectral density of the plate and cylinder oscillations; and (d) corresponding phase portraits $y_p^* - y^*$, for $k_{p1} = 0.034\text{N} \cdot \text{m/rad}$, $k_{p3} = 0.598\text{N} \cdot \text{m/rad}$ and $k_{p4} \to \infty$. The selected cases and reduced velocity are $U^* = 5.3$ (1-3) and $U^* = 9.0$ (4-6), for torsional stiffness k_{p1} (1,4), k_{p3} (2,5) and k_{p4} (3,6). Note that in (d) x-axis and y-axis marks are identical for each phase portrait. The Strouhal value for each corresponding reduced velocity has been included in (c) by black dashed lines.

guided by the plate's oscillations, as shown by the relative amplitude $\hat{A}_p^*$ shown in Fig. 5(b1). Note that the amplitude response of the plate is considerably larger as its maximum value equals $\hat{A}_p^* \simeq 0.7$, while $\hat{A}^* \simeq 0.2$.

Stappenbelt [14] reported similar responses for short rigid splitter plates, where large amplitude response ends at the end of the VIV lock-in range.

The increase of the torsional stiffness k_p weakens progressively the relative amplitude of the plate's oscillations, as shown in Fig. 5(b1). This attenuated dynamics alters the coupled dynamic response of the cylinder-plate system depicted in Fig. 5(a1). As observed, the weakest response is featured by k_{p2}, for which the oscillations are nearly nil over the whole range of U^* as already discussed in the previous Sect. III B.

On the other hand, the response for k_{p3} is also very weak, although slightly less attenuated than that corresponding to the reference k_{p2} case. In particular, the response is amplified at very low values of U^* when compared to the plain cylinder. This mild oscillation continues along the former initial branch, but it vanishes around $U^* \simeq 6$, from where the response practically disappears.

Interestingly, the system with the rigid splitter plate, i.e. $k_{p4} \to \infty$, displays also an overall attenuated response, although the oscillations of the system are amplified for small and large values of reduced velocity, thus defining two distinct regions of response.

When the frequency of the system is analyzed with help of Fig. 5(a2), it is observed that these two regions identified for large stiffness k_{p3} and k_{p4} are respectively related to similar frequency responses. In particular, at low U^*, the system oscillations are guided by a linearly increasing frequency ratio f^*, following approximately the shedding frequency. In general, this linear trend lies slightly below the shedding law of the plain cylinder $St \cdot U^*$,

Accepted to Phys. Fluids 10.1063/5.0184410

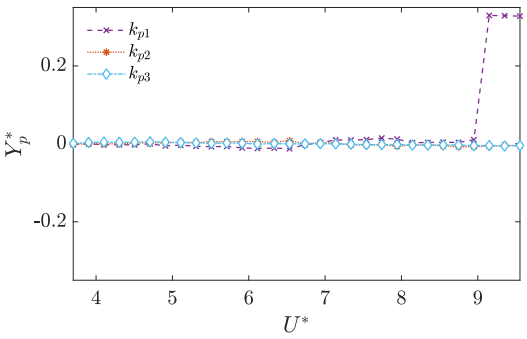

FIG. 7. Mean tip displacement Y_p^* of the $l^* = 2$ plate for different torsional stiffness.

what may be due to the increased hydrodynamic inertia (with the transverse motions) of the cylinder-plate system. Additionally, at high U^*, the frequency response displays nearly constant ratios of $f^* \simeq 0.4$, what again might be an indication of beginning of galloping-like response, which is particularly evident in the case of $k_p \to \infty$, as the value of $\hat{A}^*$ rises monotonously at large U^*. This behaviour mimics that reported in Assi, Bearman, and Kitney [25] for rigid splitter plates. For all the hinged $l^* = 2$ plates, the shear layers wrap around the plate alternatively, which provokes a new mechanism of flow excitation under these configurations. The different obtained responses depend on how the flow forcing is sunk by the different employed flexible joints, as will be discussed in Sects. IV and V. Finally, note that the plate's relative oscillations shown Fig. 5(b2), display similar frequency responses than that of the cylinder, especially for k_{p3}.

Again, the coupled dynamics is further analyzed in terms of the flapping process of plates of different torsional stiffness and its phase with respect to the cylinder's vibration. Thus, Fig. 6 displays the flapping of plates and the cylinder motion (a), time-series of cylinder y^* and plate's tip y_p^* displacement (b), corresponding PSD (c) and phase portraits (y_p^*, y^*) (d), for reduced velocity values of $U^* = 5.3$ (1-3) and $U^* = 9.0$ (4-6), and torsional stiffness $k_{p1} = 0.034\text{N} \cdot \text{m/rad}$, $k_{p3} = 0.598\text{N} \cdot \text{m/rad}$ and $k_{p4} \to \infty$. Note that case $k_{p2} = 0.092\text{N} \cdot \text{m/rad}$, is represented in Fig. 4, and denoted as $l^* = 2$.

First, as expected from the previous discussion on $\hat{A}^*$ and $\hat{A}_p^*$, the lowest value of torsional stiffness k_{p1} displays the largest relative flapping amplitude (Fig. 6a1, b1), which grows with the reduced velocity. The cylinder's vibration is however less intense, and both oscillating histories of cylinder and plate are seen to be out-of-phase for both values of the reduced velocity $U^* = 5.3$ (Fig. 6b1, d1) and 9.0 (Fig. 6b4, d4). As inferred from Fig. 5, the dominating frequencies of both the plate and cylinder oscillations are the same, and increase with U^*. This fact leads to phase portraits which display close circular orbits characteristic from periodic or quasi-periodic dynamics (note that for $U^* = 9.0$, there is some modulation on the amplitude of the time-series, what translates into a stronger meandering of the orbits).

As the torsional stiffness increases, the flapping amplitude weakens, as illustrated in Fig. 6(a2, a5) and (b2, b5) for k_{p3}. It is observed that the cylinder and plate oscillates approximately in phase and with the same frequency (Fig. 6 c2, c5). As a consequence, the phase diagrams show traces developing approximately along the bisector diagonal. The irregularity of the portraits shape is the outcome of the erratic weak oscillating signals of the plate and cylinder, which is especially evident for $U^* = 9.0$. Finally, for the static rigid plate, i.e. $k_{p4} \to \infty$, the amplitude of plate's displacement is obviously close to zero in Fig. 6(a3, a6) and (b3, b6), being the weak, irregular vibration simply related to the experimental noise, as we are characterizing the motion of the plate with respect to the cylinder displacement. Consequently, the phase portrait display horizontal shapes associated to sole vibrations of the cylinder y^* (along the abscissa axis).

Finally, once the oscillating dynamics of the system has been discussed, let us analyzed

Accepted to Phys. Fluids 10.1063/5.0184410

the mean position of the plates. As reported by Cimbala and Garg [21] for free-to-rotate cylinders with fixed splitter plates, or similarly, by Assi, Bearman, and Kitney [25] and Gu *et al.* [24] for free-to-rotate splitter plates mounted in cylinders, these multibody systems may perform rotary oscillation around asymmetric deflected positions that are the outcome of bi-stable equilibrium of the fluid-structure interaction coupling. In view of the similarities between those systems and that of the hinged plate presented here, we analyze, with help of Fig. 7, the evolution of the mean position of the $l^* = 2$ plate, given by the mean tip displacement, $Y_p^* = Y_p/D$, against U^*, for the three values of torsional stiffness k_p. It can be observed that the location of k_{p2} and k_{p3} are approximately centred, i.e. $Y_p^* \simeq 0$. Interestingly, the most flexible joint, k_{p1}, features also a centred location for $U^* \leq 9.0$, however, above that threshold, a divergence occurs and Y_p takes a constant value of 0.32 hereinafter. Such asymmetric deflection of the most flexible plate leads to the complete attenuation of the oscillating dynamics, as shown in Fig. 5. The attenuation of the VIV response was also reported by Assi, Bearman, and Kitney [25] for a free-to-rotate plate. It was also shown by Gu *et al.* [24] that the asymmetric deflection of the plates entails the decrease in the fluctuating lift.

That said, the implementation of hinged splitter plates has been shown to lead to mitigated or partially suppressed oscillations over a wide range of reduced velocity, with the cylinder responding differently depending on the length of the plate or the torsional stiffness of the flexible joint. This controlled dynamics will be subsequently analyzed based on the force coefficients and the phase difference between the forcing and the response, together with the flow visualization of the near wake for selected representative cases, which will also help shedding some light on the control mechanisms acting here.

IV. FLOW VISUALIZATIONS

Once the dynamic response of the system has been discussed, we present next the results from the flow visualizations undertaken for selected cases. The flow visualizations have been performed for those configurations which better explain the observed differences on the dynamic response. More precisely, the experiments have been performed for the fixed cylinder, the free-to-vibrate plain cylinder and two cylinder-plate arrangements with length $l^* = 2$, namely two different joint stiffness, k_{p2} and k_{p4}.

Figs.(8 - 11) present the shedding process by means of phase-averaged dimensionless spanwise vorticity contours (note that $w^* = wD/u_\infty$, where w is the spanwinse vorticity) and flow streamlines at $U^* = 5.3$ ($Re \simeq 7000$). Eight selected phases, from 0 to $7\pi/4$, have been averaged using the cylinder subsequent positions during at least 20 shedding cycles. Here, the 0 phase corresponds to the instant where the cylinder position crosses from $y^* < 0$ positions to $y^* > 0$ ones. For the case denoted as fixed cylinder, in which the cylinder is not allowed to move, the phases are obtained from the the transversal velocity (v^*) temporal evolution at ($x^* = 2.5$, $y^* = 0$), here also, the 0 phase corresponds to the instant where the transversal velocity goes from $v^* < 0$ values to $v^* > 0$ ones.

A. Flow around the plain cylinder

In this section, we compare the fixed circular cylinder wake dynamics with that of the free-to-vibrate plain cylinder. In the first case, the measured flow represents the canonical vortex shedding in the wake behind a fixed cylinder[31]. As it can be seen in Fig. 8, alternative vortices are formed and shed from each side of the cylinder at a given frequency, f_w. In the shedding sequence, it can be observed that the vortex formation length is around $x^* \simeq 2$, especially at 0 and $5\pi/4$ phases. This feature may be able to explain why the plate with a length $l^* = 2$ exhibits the best performance, as it alters the formation length.

On the other hand, the free-to-vibrate plain cylinder vortex shedding sequence is illustrated in Fig. 9 at $U^* = 5.3$. This reduced velocity corresponds to the maximum cylinder

Accepted to Phys. Fluids 10.1063/5.0184410

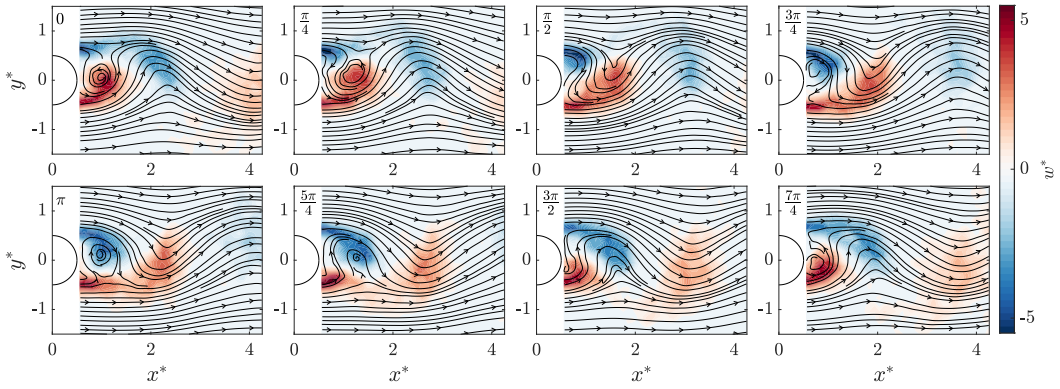

FIG. 8. Phase-averaged spanwise vorticity (w^*) contours and flow streamlines over one cycle of shedding for the fixed plain cylinder case at $Re \simeq 7000$. The corresponding phase-averaged positions of the cylinder have been plotted in different panels to better illustrate the shedding process.

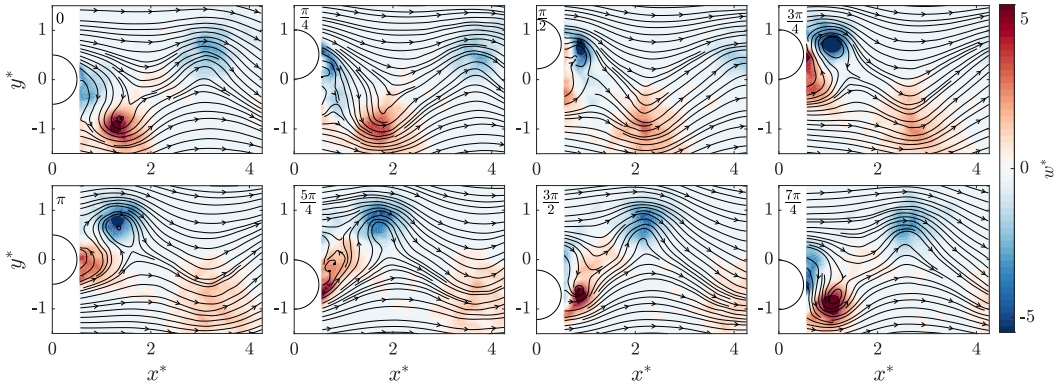

FIG. 9. Phase-averaged spanwise vorticity (w^*) contours and flow streamlines over one cycle of shedding for the free-to-vibrate plain cylinder case at $U^* = 5.3$.

response on the upper branch. Figure 9 depicts that the cylinder displacement induces a greater rotation in the flow, forming stronger vortices (with higher associated vorticity) that may produce higher transverse forces. In addition, the core positions of the shed vortices are displaced far away from the cylinder center, reducing the importance of the recirculation region in this flow configuration.

B. Effect of the torsional joint stiffness on the near wake

Now, we focus on the interaction between the tested splitter plates and the forming wake. In order to analyze the role of the flexible silicone in the fluid-structure mechanisms, we have performed experiments for a fixed plate length $l^* = 2$ and two different joint stiffness, k_{p2} and k_{p4}. In the tested cylinder-plate arrangements, the separated shear layers wrap around the plate alternatively (see Figs. 10 and 11). However, for the rigid plate, k_{p4}, the wake excitation has to go directly to the cylinder (and to the springs on the low mass-damping system), causing a stronger cylinder's response. When we introduce the silicone rubber, the wake excitation can be absorbed by the torsional joint, reducing the magnitude of the forcing transferred to the cylinder. As mentioned above, it can be noticed that the control effect of the hinged plate is particularly important for this plate's length ($l^* = 2$) since the recirculation regions formed at each side of the plates have a $\simeq 2D$ extension (see Figs. 10 and 11). In addition, the formation of a tip vortex can be observed for the rigid plate k_{p4}

Accepted to Phys. Fluids 10.1063/5.0184410

(see Fig. 11) at $\pi/4$ or $3\pi/2$ phases, in contrast to the plate k_{p2}, where it cannot be noticed (see Fig. 10). This effect may be associated to the ability of the hinged plate to adapt to the flow, which contributes to reduce the wake forcing on the cylinder-plate system.

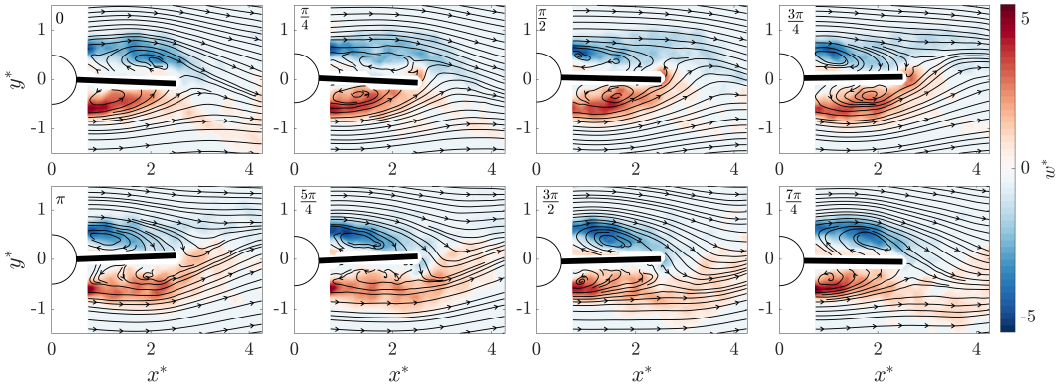

FIG. 10. Phase-averaged spanwise vorticity (w^*) contours and flow streamlines over one cycle of shedding for the k_{p2} cylinder-plate arrangement case at $U^* = 5.3$. Note that the corresponding phase-averaged positions of the cylinder and the plate have been included to better illustrate the shedding process.

Finally, Fig. 10 shows that the degree of freedom introduced with the flexibility of the torsional joint allows to reduce the transversal velocity on the wake in comparison with the rigid plate (see Fig. 11), which may in turn reduce the wake excitation. Following this idea, we can compute the integral wake transversal velocity, $\tilde{v}$, at a given streamwise position as, $\tilde{v}(t^*) = \langle v(y^*, t^*) \rangle$, where $\langle\rangle$ represents spatial averaging.

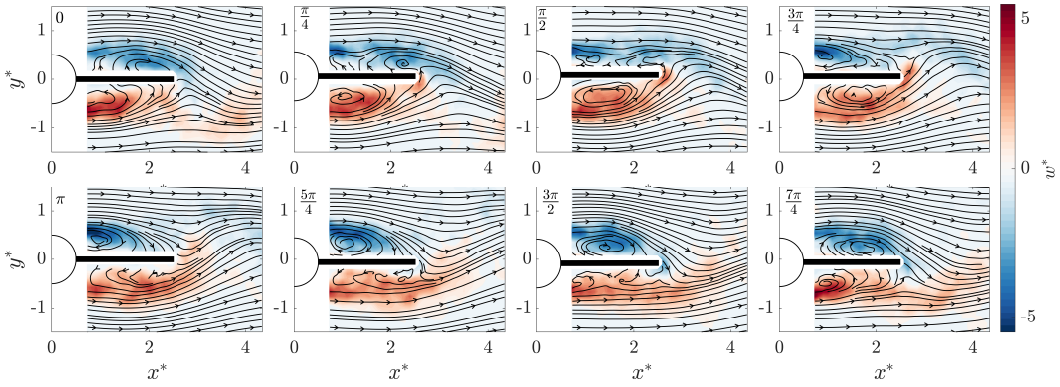

FIG. 11. Phase-averaged spanwise vorticity (w^*) contours and flow streamlines over one cycle of shedding for the k_{p4} cylinder-plate arrangement case at $U^* = 5.3$. Note that the corresponding phase-averaged positions of the cylinder and the plate have been included to better illustrate the shedding process.

This magnitude accounts for the instantaneous transversal velocity in the wake that may qualitatively measure the transversal wake forcing or excitation for a given near wake topology. Figure 12 represents the temporal evolution of $\tilde{v}$ for the selected phases depicted in Figs.(8 - 11) at $x^* = 3.5$ between $-1.5 \leq y \leq 1.5$. As expected, the alternative periodic shedding of vortices of the fixed and free-to-vibrate plain cylinder cases induces a strong transversal velocity in the wake. that provokes the strong cylinder response. Conversely, the integral wake transversal velocity is reduced when a splitter plate is introduced, which may explain the observed reduction on the cylinder-plate response. A comparison between the results for k_{p2} and k_{p4} reveals that $\tilde{v}$ is weaker as the stiffness is reduced. This fact may

Accepted to Phys. Fluids 10.1063/5.0184410

be attributed to the damping action of the silicone rubber, which seems to reduce the wake excitation, strongly mitigating the cylinder's response, as previously seen in Sect. III.

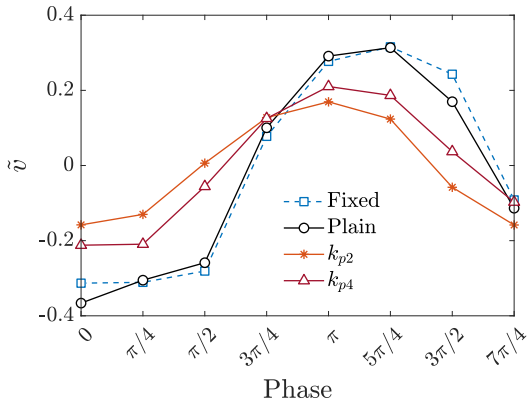

FIG. 12. Integral wake transversal velocity, $\tilde{v}$, computed at $x^* = 3.5$ for $-1.5 \leq y \leq 1.5$ at selected phases of the shedding cycle corresponding to different configurations.

V. FORCE COEFFICIENTS

A. Cross-flow force coefficient and components

The analysis of the force coefficients is next addressed. The cross-flow or lift coefficient amplitude $\hat{C}_y$ is computed as indicated in Sect. II. This coefficient can additionally divided into components in phase with the acceleration, $\hat{C}_{y,a}$, and with the velocity, $\hat{C}_{y,u}$, according to the expressions given in Jiménez-González and Huera-Huarte[32]:

$$\hat{C}_{y,a} = \frac{\sqrt{2}\,(\mathrm{f}_y - \mathrm{F}_y)}{0.5\rho D L u_\infty^2} \frac{y}{\sqrt{Y^2}}, \tag{4}$$

and

$$\hat{C}_{y,u} = \frac{\sqrt{2}\,(\mathrm{f}_y - \mathrm{F}_y)}{0.5\rho D L u_\infty^2} \frac{\dot{y}}{\sqrt{\dot{Y}^2}}, \tag{5}$$

where $\dot{y}$ is the temporal derivative of the cross-flow displacement of the cylinder, y.

These components may help interpreting, respectively, the effect of inertia and transfer of energy between fluid and structure. In particular, the positive values of $C_{y,u}$ indicate a net transfer from the fluid to the body, what excites the structural response; while the sign of $C_{y,a}$ is related to the effective added mass and phase between forcing and response[3]. In fact, to complement the analysis, the averaged phase difference, Φ, between the y displacement and the lift force, c_y, was obtained using the Hilbert transform to the temporal variable,

$$\phi = \phi_{c_y} - \phi_y. \tag{6}$$

Figure 13 depicts the amplitude of lift coefficient and corresponding components, together with the phase difference, for the different plate length l^* based on stiffness $k_{p2} = 0.096$ N·m/rad and the plain cylinder, which will be first analyzed to set a reference. For that case, the lift coefficient is shown to peak, with $\hat{C}_y \simeq 1.5$, approximately at $U^* \simeq 5.1$ (see Fig. 13a), that corresponds to the amplitude jump between initial and upper branches in Fig. 2(a). After that, there is a sudden decrease of $\hat{C}_y$ coinciding with the transition between upper

Accepted to Phys. Fluids 10.1063/5.0184410

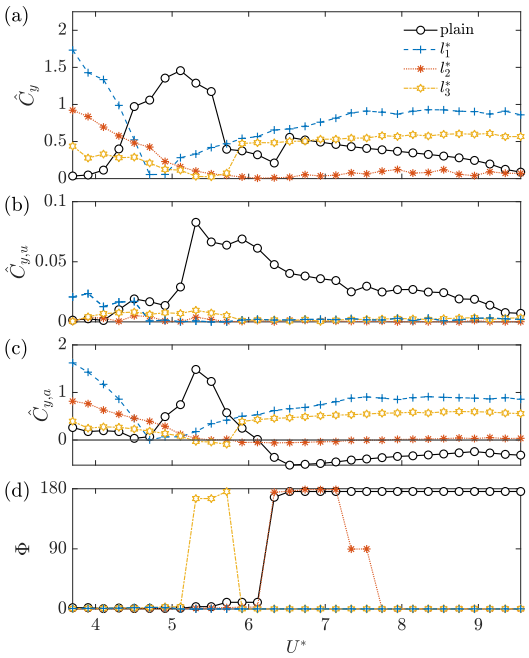

FIG. 13. Amplitude of (a) lift coefficient, $\hat{C}_y$, along with corresponding components in phase with velocity (b) and displacement (c), and phase difference between lift and $y-$displacement (d), for different plate length l^* and stiffness $k_{p2} = 0.096$ N·m/rad. A solid line has been included for $\hat{C}_{y,a}$ to illustrate the effective added mass and phase between forcing and response.

and lower branches, from which the value decays mildly with growing U^*, until reaching a nearly nil value as the VIV response decays in amplitude. The lift components in phase with velocity, $\hat{C}_{y,u}$, presents positive values for all U^*, reaching its maximum within the upper branch of amplitude response at $U^* = 5.3$. As mentioned previously, this coefficient $\hat{C}_{y,u}$ can be used to estimate the fluid damping effect and the energy transferred from the fluid to the moving structure; so that its maximum absolute value is associated to largest excitation. Besides, the component $\hat{C}_{y,a}$ features a peak at $U^* \simeq 5.3$, and decreases until reaching a negative value for $U^* > 6.0$, where the phase changes from 0° to 180° (Fig. 13d). This phase shift takes place once the system oscillating frequency reaches its natural one, i.e. $f^* \simeq 1$ (Fig. 2a2), and entails the attenuation of the amplitude response over the lower branch, as now the exciting force acts in the opposite direction to the body's motion.

The effect of mounting a rear hinged plate modifies the excitation force, and trends of coefficients are considerably different. In particular, for the plate of length $l^* = 1$, the lift coefficient amplitude is large at low values of reduced velocity U^*, and decreases with it, to reach a minimum around $U^* \simeq 5$ where the original upper branch of the amplitude response corresponding to the plain cylinder emerges. From here on, the lift amplitude starts to grow again monotonously. A similar trend is found for the inertia component $\hat{C}_{y,a}$, which is greater than that of the plain cylinder for low and high values of reduced velocity. The higher values of $\hat{C}_{y,a}$ are consistent with higher added mass, and therefore, lower frequencies at high U^{*3}. Additionally, the dynamic response of $l^* = 1$ exhibits very low values of $\hat{C}_{y,u}$, i.e. lower energy transfer, in contrast to the results of the plain cylinder (except for the lowest values of U^* investigated). As a result, the general dynamic response of the system cylinder-plate is attenuated, providing a weaker response (see Fig. 3). That said, unlike the plain cylinder, the phase difference between forcing and response does not change its value and is always 0° (Fig. 13d) over the whole range of reduced velocity investigated. This may compensate the lower energy transfer and foster the response at large reduced velocity.

Similar trends are obtained for the plate of $l^* = 3$, although the lift $\hat{C}_y$ and correspond-

Accepted to Phys. Fluids 10.1063/5.0184410

ing component $\hat{C}_{y,a}$ show a progressive decreasing amplitude at low U^*, as the length grows. It is interesting to observe that now the $\hat{C}_{y,a}$ component reaches negative values for $5 < U^* < 6$, what leads to a phase shift to 180° within such range. Altogether, this picture helps understanding the dynamic response identified in Fig. 3(a1) for $l^* = 1$ and 3 configurations, whereby the system has an enhanced vibration at low U^* (especially for the shortest plate) and attenuated vibrations over the upper and lower branches, although monotonously growing with U^*. The growing excitation with the reduced velocity is expected to lead to amplified responses beyond the upper limit of U^* studied here.

On the other hand, for the plate of $l^* = 2$ the lift and associated components show an intermediate behavior between $l^* = 1$ and 3. In particular, lift components feature maxima at lowest values of reduced velocity and decreasing amplitudes as reduced velocity grows, to reach nearly nil magnitudes for $U^* > 5$. The absence of excitation of the flow acting on the structure above $U^* = 5$ coincides with the mitigated dynamic response of the system observed in Fig. 3(a1). That said, the plate of $l^* = 2$ behaves therefore as an excellent configuration in terms of excitation, as shorter and longer plates present magnified coefficients. This better performance of the $l^* = 2$ plate may be linked to the fact that the typical vortex formation length observed for these kind of flows is around $2D$, as seen in Sect. IV. Therefore, that plate's length mitigates the interaction between shear layers, reducing the flow excitation to the system.

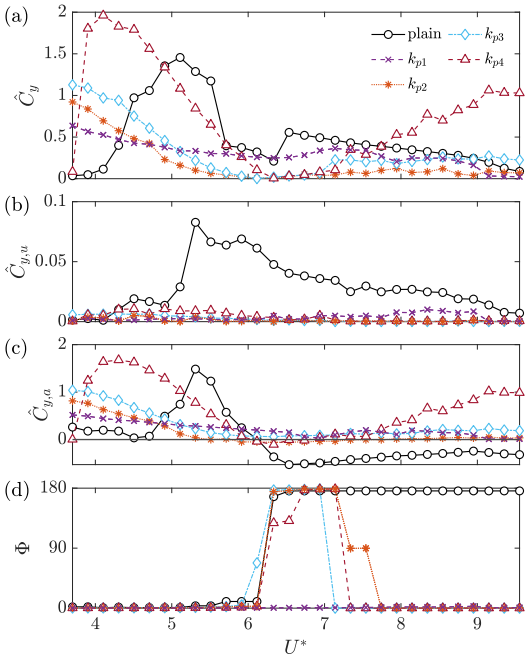

FIG. 14. Amplitude of (a) lift coefficient, $\hat{C}_y$, along with corresponding components in phase with velocity (b) and displacement (c), and phase difference between lift and $y-$displacement (d), for different values of stiffness $k_p = [k_{p1}, k_{p2}, k_{p3}, k_{p4}] = [0.034, 0.096, 0.598, \to \infty]$ N·m/rad and plate length $l^* = 2$. A solid line has been included for $\hat{C}_{y,a}$ to illustrate the effective added mass and phase between forcing and response.

The effect of the hinge torsional stiffness k_p on the lift coefficient and components is next analyzed with help of Fig. 14, where results for arrangements with $l^* = 2$ are plotted. Such variable may help estimating the capacity of adaptation of the plate to the motion of the cylinder and wake forcing. As already identified in the amplitude response for the different joints in Fig. 5, there are two distinct regions of dynamic response, at low ($U^* < 5.5$) and high ($U^* > 7$) reduced velocity respectively, which are also distinguishable for the lift coefficient in Fig. 14(a), although there are important differences between trends of

Accepted to Phys. Fluids 10.1063/5.0184410

different k_p. In particular, it is observed that, as the torsional stiffness increases, so does the value of the lift amplitude $\hat{C}_y$ at low values of the reduced velocity, being the rigid joint, i.e. k_{p4}, the case of largest excitation within the range of $3.8 \geq U^* < 5.5$, where $\hat{C}_y \simeq 2$. The excitation of the cylinder-plate system is considerably weakened between $5 < U^* < 7$, as the lift amplitude decreases abruptly, coincident with the attenuation of oscillations over the original upper branch of the plain cylinder and beginning of the lower branch. Moreover, following the vortex shedding sequences shown in Figs. 10 and 11, for different stiffness values, corresponding to k_{p2} and k_{p4} plates respectively, just at $U^* = 5.3$, a general behaviour can be inferred depending on the stiffness value. It appears that the flow topology is similar for both cases, however, while for the extreme case corresponding to a rigid plate, k_{p4}, the wake excitation has to be directly absorbed by the cylinder (and thus by the springs on the low mass-damping system), in the case of the more-flexibly-hinged plates the effect of the wake excitation is divided between the cylinder and the flexible hinge, which reduces the response of the whole system. Finally, the lift amplitude grows again at higher U^*, for all values of k_p, except for k_{p2}, for which the excitation is nearly nil, $\hat{C}_y \simeq 0$. In particular, the values of $\hat{C}_y$ of k_{p1} and k_{p3} are similar to that of the plain cylinder, whereas that of the static plate rises monotonously to reach large amplitudes of $\hat{C}_y \simeq 1$.

In spite of the large amplitudes of the lift coefficient displayed by the cylinder-plate arrangements for low and high ranges of reduced velocity, it was shown that the amplitude response is however attenuated with respect to that of the plain cylinder. That effect may be caused by the low stiffness of the flexible hinge and to the reduced wake transversal velocity induced by the hinged plates. Moreover, the component $\hat{C}_{y,u}$ is in general very small, and smaller than that of the reference case, as expected from an attenuated response and weak energy transfer from the fluid to the cylinder-plate system. In particular, the highest values of $\hat{C}_{y,u}$ of the controlled systems are displayed by the arrangement with the most flexible joint, k_{p1}, and rigid case k_{p4}, for $U^* < 6$ and $7 < U^* < 9$ respectively, just where the amplitude response of these configuration is less attenuated (Fig. 5a1).

Additionally, the trends of component $\hat{C}_{y,a}$ are very similar to that of the lift components, displaying again amplified values over the two distinct regions at low and high reduced velocities, when compared to the reference cylinder case. This again can be interpreted as an increase of the added mass, and lower response frequencies, as observed in Fig. 5. Interestingly, for k_{p1}, $\hat{C}_{y,a}$ never takes negative values, what translates into a phase difference between forcing and response of 0°, as depicted in Fig. 14(d). For the remaining cases with higher stiffness, $\hat{C}_{y,a}$ is only negative within an interval covering a $6 < U^* < 7.5$ approximately, and therefore, the shift in the phase difference from 0° to 180° is soon reverted for $U^* > 7.5$, from where the forcing and response are back in phase. As discussed earlier, the first shift has been generally identified as one of the characteristics of lock-in in VIV of a plain cylinder[13], whereas the subsequent drop to small values of Φ are an indication of the beginning of galloping-like responses[15].

B. Spectral analysis of the cross-flow forcing

In general, in view of the previous results, two types of responses have been identified for the cylinder-plate assembles. In particular, depending on the plate's length and torsional stiffness of the joint, a VIV regime featuring small-amplitude oscillation may develop at low values of U^*, over the initial branch of response; while galloping-like responses can be triggered at high U^*.

Following the latter observation, we will next discuss these different regimes in terms of the forcing frequency, provided by the spectral analysis of the lift coefficient, c_y. Thus, Fig. 15 displays PSD spectra from cross-flow force signals along with their corresponding dominant forcing and oscillation frequencies, for the plain cylinder case (Fig. 15a) and controlled configurations of different lengths (Fig. 15, b-d) and torsional stiffness (Fig. 15

Accepted to Phys. Fluids 10.1063/5.0184410

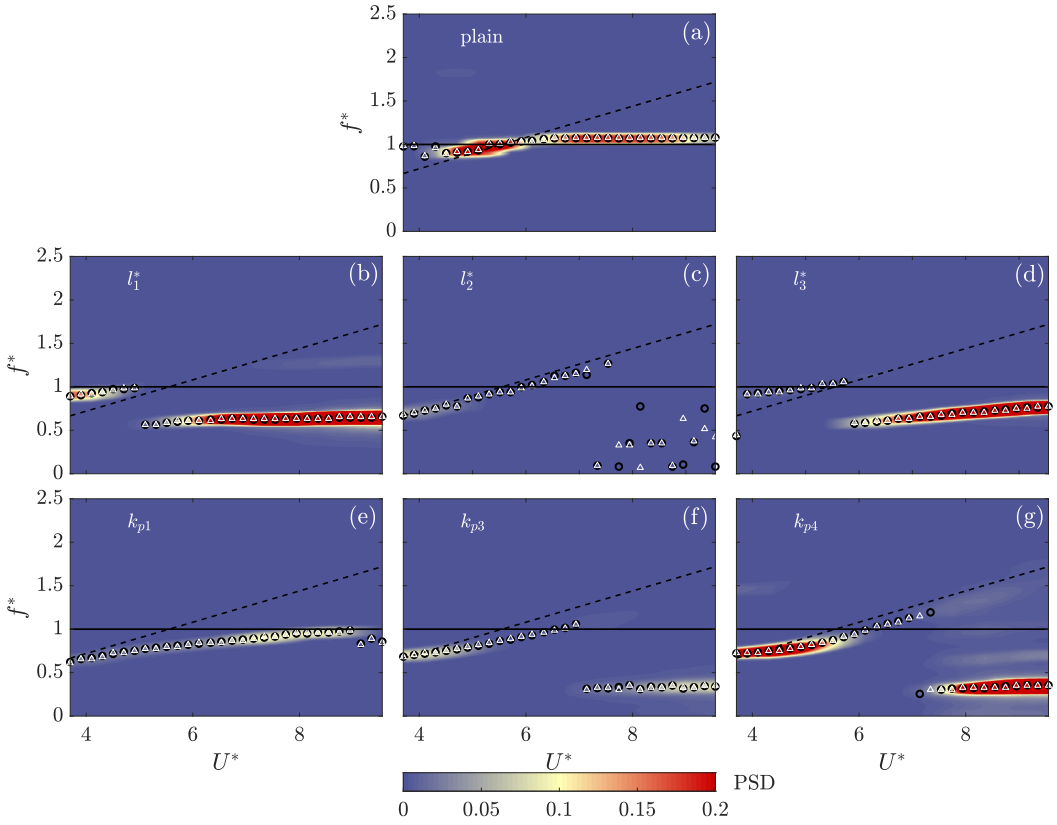

FIG. 15. PSD spectra of cross-flow force signals, c_y depicted by background contours and corresponding dominant forcing frequency (white triangle symbols) and response oscillation frequency (black circles) for plain cylinder (a, top row) and controlled configurations: with plates of length (medium row) $l^* = 1$ (b), 2 (c) and 3 (d), for intermediate value of the torsional stiffness k_{p2}; with torsional stiffness (bottom row) k_{p1} (e), k_{p3} (f) and k_{p4} (g), for a fixed plate of length $l^* = 2$. Dashed lines represent the Strouhal law with $St \simeq 0.18$, the colormap indicates value of PSD amplitude of cross-flow force and the solid line is $f^* = 1$.

c,e-g). Power spectra are used here to qualitatively estimate the intensity of wake oscillations and coherence of vortex shedding. In general, the response frequency is coincident with the dominant forcing frequency for the whole range of reduced velocity investigated and different configurations, showing a strong coupling as the flow and the solid dynamics are highly synchronized.

The plain cylinder case is characterized by three intervals of forcing. Thus, the initial branch displays frequencies that follow approximately the Strouhal law, until a point where the oscillations in the wake attain its largest magnitude, from which frequencies start to level off, with $f^* = 1$ thus marking the beginning of the upper branch. For $U^* \simeq 6$, the magnitude of PSD decreases, a known feature of the transition region between upper and lower branches[30]. From here on, the dominant frequencies reach a plateau at $f^* \geq 1$ (as it typically occurs for flexibly mounted cylinders with low mass ratios). At the lower branch, the magnitude of PSD decreases and more periodic spectra with thinner peaks are observed[30].

The effect of installing a flexibly-hinged plate is evident in terms of frequency forcing and spectral amplitude, as observed in Fig. 15(b-g). Let us begin the discussion on the effect of the increasing torsional stiffness k_p for a constant plate's length. In particular, as observed in Fig. 15(e) for the most flexible joint of k_{p1}, the excitation is guided by an increasing frequency which follows approximately a linear trend, until reaching the value of $f^* = 1$,

Accepted to Phys. Fluids 10.1063/5.0184410

from which the spectral amplitude becomes nearly indiscernible, and the frequency decreases below $f^* = 1$, although its value remains close to it. As detailed in Sahu, Furquan, and Mittal [20] and observed in our PIV measurements, the frequency of the shedding guiding the VIV regime decreases with the addition of plates, as so does the spacing between the vortices when compared to the original cylinder wake. Besides, the drop in frequency at $U^* = 9.0$, is shown to be associated to a discontinuity or *kink* in the trend of amplitude response in Fig. 5(a1), similar to that reported, e.g. by Bearman *et al.* [33] for squared cylinders. This behavior is generally attributed to interaction between VIV and galloping-like responses. In fact, as shown in Fig. 14(d), no change in phase difference is observed and $\Phi = 0°$ over the whole range of U^* studied here.

As the stiffness of the joint increases, the range of reduced velocity for which the VIV regime (resp. galloping-like) is active narrows (resp. widens) progressively, as it can be inferred from Fig. 15(c), (f) and (g), which represent respectively k_{p2}, k_{p3} and k_{p4}. Interestingly, the forcing frequency features are very similar for the three values of stiffness, with the transition between VIV and galloping-like regimes being set around $U^* = 7.0$. This transition between regimes is clearly identified in the phase difference diagram of Fig. 14(d) with corresponding shifts from 180° to 0°, and occurs when the vibration frequency crosses the natural frequency of the system[34]. There are however notable differences in terms of spectral amplitude, i.e. excitation magnitude. Thus, excepting for the preferred case of k_{p2} for which the vibrations are mitigated and no coherence is found for the forcing frequency at high U^*, it is seen that increasing the stiffness beyond such a best-performing value of k_{p2}, rises the cross-flow force energy over both VIV and galloping-like regimes, being it maximum for the rigid static plate. This is in line with Fig. 12, the k_{p4} case, the integral wake transversal velocity is higher than in the k_{p2} case, which may indicate a greater excitement in the wake, possibly justifying the higher response of the cylinder.

On the other hand, the effect of varying the plate length while keeping constant the stiffness, i.e. k_{p2}, may produce similar excitation to that provided by the increasing stiffness, as illustrated in Fig. 15(b,d), where both VIV and galloping-like regimes are clearly distinguishable, as in Fig. 15 (g). In particular, the shortest plate $l^* = 1$ displays intense spectral amplitude along the initial branch, which excites the system close to the natural frequency, thus leading to amplified vibrations along the initial branch in Fig. 3(a1). When the forcing frequency reaches the value of $f^* \simeq 1$, there is a transition towards the galloping-like regime, characterized by a constant and low forcing frequency and strong spectral magnitude. The dynamic behaviour is very similar to that of the static $l^* = 1$ plate analyzed in Assi and Bearman [13], and it might be attributed to the fact that the plate lies inside the vortex formation length (see Figs. 8, 9), therefore it is weakly excited by the shedding.

When the plate's length is increased to $l^* = 3$, above the more suitable case of $l^* = 2$, the VIV regime at low reduced velocity is less intense and extends now up to $U^* \simeq 6.0$. From here, the new regime at high U^* displays again a forcing frequency $f^* < 1$ which increases now slightly with U^*, with a slope that is approximately $0.5St \cdot U^*$. This slowdown of the forcing with some degree of synchronization with the behavior of the Strouhal law, is presumably consequence of the strong flapping process (see Fig. 3b1) which now guides the shedding.

C. Drag coefficient

Finally, we will evaluate the effect of control plates on the mean drag coefficient, C_x. Figure 16 displays the time-averaged drag coefficient C_x as a function of the reduced velocity for controlled systems with different plate's length l^* for a constant stiffness k_{p2}(a) and different torsional stiffness k_p for a constant $l^* = 2$(b), along with the plain cylinder case, which is shown for comparison. In general, for the uncontrolled case, the drag coefficient is sensitive to the branches of the amplitude response (see Figs. 3 and 5) displaying larger values along the upper branch, where the response is highest, and showing lower values at initial and lower branches, where the value is similar to those typically reported for static

Accepted to Phys. Fluids 10.1063/5.0184410

cylinders, at the same Re.

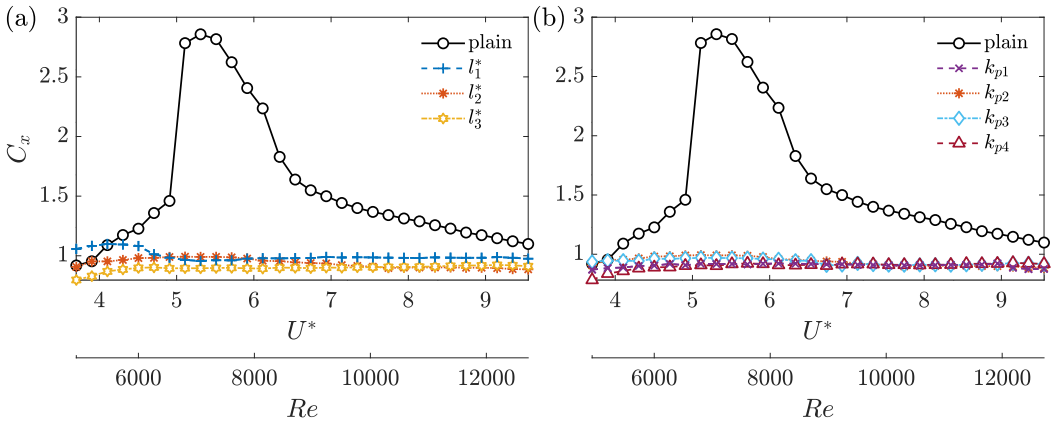

FIG. 16. Time-averaged drag coefficient for different configurations of the cylinder and plate system: (a) effect of the plate's length l^* for constant k_{p2} and (b) effect of the torsional stiffness of the joint k_p for a constant $l^* = 2$.

In general, the addition of a rear plate reduces dramatically the magnitude of the mean drag, which now displays nearly constant values for all configurations between 0.9 and 1. In order to identify the relationship between the measured force coefficient and the near wake features, time averaged flow fields for the fixed cylinder case and a cylinder-plate arrangement (l_2^*, k_{p2}) at $U^* = 5.3$ ($Re \simeq 7000$) are depicted in Fig. 17. It can be noticed that the presence of the plate is seen to separate the two recirculating cores of the near wake and to induce the elongation of the recirculation region, giving rise to the drag reduction as a consequence of the strong streamlining of the wake, as pointed out by Apelt, West, and Szewczyk [12].

Thus, it is seen that, in general, increasing the length of the plate (Fig. 16a) translates into slight reductions of C_x within the range of U^* studied herein. Some small differences associated to the dynamic behavior of the system are however discernible. For instance, at low U^* the drag of the arrangement with $l^* = 1$ increases on account of the amplified response of the system, mainly due to the widening of the wake transverse extension induced by the presence of a rear plate. This fact can be observed in the comparison of the average velocity contours shown in Fig. 17. Such an effect may become important for conditions of low values of U^* and small l^*, under which the shear effect due to the stream, barely elongates the recirculation region, being l^* not long enough to maintain the flow attachment. Similarly, the amplified oscillations of the system with $l^* = 3$ for high values of U^* increases somewhat the mean drag above that of $l^* = 2$.

Regarding the effect of the torsional stiffness k_p, little differences are found among the cases, if only, the static plate provides with lower values of drag, on account of the nonexistent flapping of plates, which has been shown to decrease the pressure in the near wake of bluff bodies[35] and to increase the velocity magnitude inside the recirculation region. Lastly, it is interesting to note that, the stable steady deflection of the plate with k_{p1} for $U^* > 9.0$ translates into a very slight reduction of the mean drag.

VI. CONCLUSIONS

We have experimentally analyzed the flow-induced vibrations of a circular cylinder controlled with a flexibly-hinged splitter plate subject to uniform cross-flow. In particular, two parametric studies are included in order to characterize the effect of the control device with respect to the isolated plain cylinder case. First, three different lengths have been tested, namely $l^* = L_p/D = [1, 2, 3]$, for a given torsional stiffness of the joint k_p. Second,

Accepted to Phys. Fluids 10.1063/5.0184410

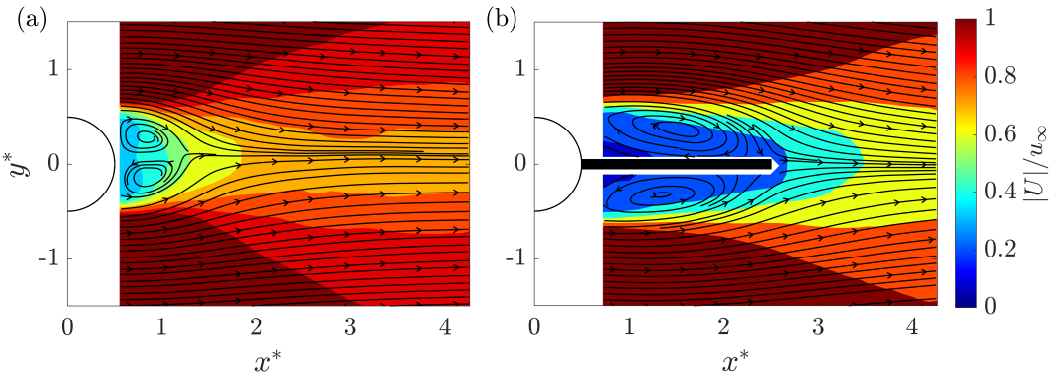

FIG. 17. Time averaged velocity magnitude contours along with flow streamlines for (a) fixed plain cylinder case and (b) k_{p2} cylinder-plate arrangement of $l^* = 2$ at $U^* = 5.3$ ($Re \simeq 7000$).

keeping constant the length of the plate to $l^* = 2$, four different values of the torsional stiffness are tested $k_p = [0.034, 0.096, 0.598, \infty)$ N · m/rad, where $k_p \to \infty$ represents the rigid case. In general, it is found that the introduction of the hinged plate can suppress the cylinder vibration and reduce the drag force at low and medium U^*. For high values of the reduced velocity, beyond the range herein investigated, the plain cylinder can perform better as galloping-type responses are reported when the plates are installed. Reductions of the dynamic response of more than 90% can be generally reached at the upper branch, especially when a plate of $l^* = 2$ with intermediate degree of torsional stiffness is attached, which is shown to represent the most effective solution as it mitigates the oscillations of the system for the whole range of U^* investigated.

More specifically, variations on the lengths and stiffness of the joint are associated to different coupled dynamics of the system and different near wake topologies. The dynamic responses of the different arrangements of cylinder and hinged plate are not alike that of the plain cylinder (characterized by the classical initial, upper and lower branches), and show two distinct regimes, whereby the dynamics at low values of reduced velocity are characterized by a modified VIV response, whereas for high values of U^* the dynamics feature galloping-like responses. In general, the response is shown to be strongly synchronized with the cross-flow forcing dynamics, especially in terms of characteristic frequencies. Thus, the VIV responses are in any case attenuated and show mild oscillations guided by an increasing shedding frequency, until the ratio $f^* > 1$, for which a general transition to galloping-like dynamics, characterized by $f^* < 1$ occurs. Transition between regimes are associated to shifts in the phase difference between the forcing and response, which typically retrieves the value of 0° when the galloping dynamics establishes.

The roles of the torsional stiffness of the joint and length are key, as demonstrated by the large attenuation provided by $l^* = 2$ and intermediate value of k_p. In particular, it has been inferred from the flow measurements that, such a length value lies around the vortex formation length typically observed for the tested Re range. This fact together with the ability of the plate to mildly adapt to flow changes lead to a reduction of the system excitation through the inhibition of the interaction between the shear layers developed in both sides of the cylinder.

Thus, using the same length, it has been shown that stiffer joints may promote the emergence of galloping-like responses for high values of the reduced velocity, thus mimicking the response of rigid plates[15,20]. Conversely, a more flexible joint (lower value of k_p) extends the prevalence of an attenuated VIV response to high U^*, and postpone the emergence of a galloping like-response.

The previous scenario can be affected by the change of the plate length. Thus, it is seen that the shortest plate of $l^* = 1$ excites the synchronization VIV response at low values of U^*, and behaves like a static plate, while it may promote unstable oscillations of the system

Accepted to Phys. Fluids 10.1063/5.0184410

at high U^*, behaving in a similar manner to a static plate[27]. In fact, this plate length lies inside the measured recirculating bubble behind the cylinder, and therefore is less exposed to changes in pressure given by the shedding, thus reducing its capability to adapt passively its position to flow changes. Conversely, the longest plate of $l^* = 3$, is clearly subject to enhanced oscillations at high U^* (where the nondimensional flexibility of the system increases), due to its larger surface and stronger interference with the wake, what promotes a progressive amplification of the response of the system at high U^*. Interestingly, although the oscillating dynamics is characterized by a frequency ratio $f^* < 1$, the frequency is seen to increase linearly with U^*, as if the dynamics is guided by the slower shedding provoked by the flapping.

Besides, it has been shown that, a certain level of torsional stiffness is required to correct potential asymmetric mean positions of the hinged plate. In particular, this departure from the symmetric location has been only observed for the most flexible case of $k_{p1} = 0.034$ N $\cdot$ m/rad. This stable departure from the centred location is reminiscent from the steady bifurcation reported by Cimbala and Garg [21] and Gu *et al.* [24] for rotary plates around the static cylinder, and the elastically-mounted cylinder[25]. The steady mode is shown therein to reduce the excitation of the system, which has been also confirmed here.

Finally, when compared to flexible plates[18] or rigid plates[15], as control devices for VIV, the hinged plates display intermediate behavior between these two configurations, where the complete suppression of VIV or the excitation of galloping-like responses can be either promoted, depending on the capacity to adapt to flow changes that is given by the plate length and torsional stiffness. In all plate cases, the shear layers are seen to wrap around the plate alternatively. However, while for the rigid plate, k_{p4}, the wake excitation has to go directly to the cylinder (and to the springs on the low mass-damping system), in the case of the flexibly-hinged plates, the wake excitation is divided between the cylinder and the silicone rubber.

In summary, the use of hinged plates has been proven to provide with a significant attenuation of the VIV amplitude and drag reductions, a feature that can be considered of practical relevance in many engineering applications. The selection of parameters, such a torsional stiffness and plate length is however a key aspect to promote different controlled dynamic responses, whereby the excitation can lead to galloping-like responses in some cases. The obtained results allow to perform a more detailed study where additional plate's lenghts can be tested. Morever, a deeper analysis on the fluid-structure mechanism behind the forcing transfer between the flow and the cylinder-plate system can be adressed. Finally, a multi-body response model can be adapted to the problem in order to analyze which part of the wake excitation is sunk by the flexible hinge or by the system's springs. These features can be also of interest for practical systems where energy harvesting is envisaged.

ACKNOWLEDGEMENTS

This work has been financed by the Junta de Andalucía, Universidad de Jaén, and European Funds under Project FEDER-UJA 1262764. This work is also a result of the Projects TED2021-131805B-C21 and TED2021-131805B-C22 financed by the Spanish MCIN/ AEI/ 10.13039/501100011033/ and the European Union NextGenerationEU/PRTR. M.L.D. also acknowledges the support from Grant FJC2020-043093-I funded by MCIN/ AEI/ 10.13039/501100011033 and, as appropriate, by "ESF Investing in your future" or by European Union NextGenerationEU/PRTR. Finally, J.C.M.H. acknowledges for the support of the Spanish MECD through FPU20/07261.

REFERENCES

[1]R. Blevins, *Flow-Induced Vibration, 2nd Edition* (Van Nostrand Reinhold, 1990).

Accepted to Phys. Fluids 10.1063/5.0184410

[2]B. Sumer and J. Fredsoe, *Hydrodynamics around cylindrical structures*, Advanced Series on Ocean Engineering, Vol. 26 (World Scientific, 1997).

[3]C. Williamson and R. Govardhan, "Vortex-induced vibrations," Annu. Rev. Fluid Mech. **36**, 413–455 (2004).

[4]P. Bearman, "Circular cylinder wakes and vortex-induced vibrations," J. Fluids Struct. **27**, 648–658 (2011), IUTAM Symposium on Bluff Body Wakes and Vortex-Induced Vibrations (BBVIV-6).

[5]M. M. Zdravkovich, "Review and classification of various aerodynamic and hydrodynamic means for suppressing vortex shedding," J. Wind Eng. Ind. Aerod. **7**, 145–189 (1981).

[6]P. Bearman, "Vortex shedding from oscillating bluff bodies," Annu. Rev. Fluid Mech. **16**, 195–222 (1984).

[7]T. Sarpkaya, "A critical review of the intrinsic nature of vortex-induced vibrations," J. Fluids Struct. **19**, 389–447 (2004).

[8]H. Choi, W. Jeon, and J. Kim, "Control of flow over a bluff body," Annu. Rev. Fluid Mech. **40**, 113–139 (2008).

[9]Y. Nakamura, K. Hirata, and K. Kashima, "Galloping of a circular cylinder in the presence of a splitter plate," J. Fluids Struct. **8**, 355–365 (1994).

[10]J.-s. Wang, D. Fan, and K. Lin, "A review on flow-induced vibration of offshore circular cylinders," J. Hydrodyn. **32**, 415–440 (2020).

[11]M. Païdoussis, S. J. Price, and E. De Langre, *Fluid-structure interactions: cross-flow-induced instabilities* (Cambridge University Press, 2011).

[12]C. J. Apelt, G. S. West, and A. A. Szewczyk, "The effects of wake splitter plates on the flow past a circular cylinder in the range $10^4 < Re < 5 \times 10^4$," J. Fluid Mech. **61**, 187–198 (1973).

[13]G. R. Assi and P. W. Bearman, "Transverse galloping of circular cylinders fitted with solid and slotted splitter plates," J. Fluids Struct. **54**, 263–280 (2015).

[14]B. Stappenbelt, "Splitter-Plate Wake Stabilisation And Low Aspect Ratio Cylinder Flow-induced Vibration Mitigation," Int. J. Offshore Polar Eng. **20** (2010).

[15]L. Zeng, F. Zhao, H. Wang, Y. Liu, and H. Tang, "Control of flow-induced vibration of a circular cylinder using a splitter plate," Phys. Fluids **35**, 087104 (2023).

[16]T. R. Sahu, M. Furquan, Y. Jaiswal, and S. Mittal, "Flow-induced vibration of a circular cylinder with rigid splitter plate," J. Fluids Struct. **89**, 244–256 (2019), Bluff Body Wakes and Vortex-induced Vibrations (BBVIV-7).

[17]G. P. Cui and L. H. Feng, "Suppression of vortex-induced vibration of a circular cylinder by a finite-span flexible splitter plate," Phys. Rev. Fluids **7**, 024708 (2022).

[18]G. P. Cui, L. H. Feng, and Y.-W. Hu, "Flow-induced vibration control of a circular cylinder by using flexible and rigid splitter plates," Ocean Eng. **249**, 110939 (2022).

[19]S. Liang, J. Wang, B. Xu, W. Wu, and K. Lin, "Vortex-induced vibration and structure instability for a circular cylinder with flexible splitter plates," J. Wind Eng. Ind. Aerod. **174**, 200–209 (2018).

[20]T. R. Sahu, M. Furquan, and S. Mittal, "Numerical study of flow-induced vibration of a circular cylinder with attached flexible splitter plate at low Re," J. Fluid Mech. **880**, 551–593 (2019).

[21]J. M. Cimbala and S. Garg, "Flow in the wake of a freely rotatable cylinder with splitter plate," AIAA Journal **29**, 1001–1003 (1991), https://doi.org/10.2514/3.10692.

[22]L. Lu, X.-l. Guo, G.-q. Tang, M.-m. Liu, C.-q. Chen, and Z.-h. Xie, "Numerical investigation of flow-induced rotary oscillation of circular cylinder with rigid splitter plate," Phys. Fluids **28**, 093604 (2016).

[23]S. Shukla, R. Govardhan, and J. Arakeri, "Flow over a cylinder with a hinged-splitter plate," J. Fluids Struct. **25**, 713–720 (2009), Bluff Body Wakes and Vortex-Induced Vibrations (BBVIV-5).

[24]F. Gu, J. Wang, X. Qiao, and Z. Huang, "Pressure distribution, fluctuating forces and vortex shedding behavior of circular cylinder with rotatable splitter plates," J. Fluids Struct. **28**, 263–278 (2012).

[25]G. Assi, P. Bearman, and N. Kitney, "Low drag solutions for suppressing vortex-induced vibration of circular cylinders," J. Fluids Struct. **25**, 666–675 (2009), Bluff Body Wakes and Vortex-Induced Vibrations (BBVIV-5).

[26]G. R. Assi, P. W. Bearman, and M. A. Tognarelli, "On the stability of a free-to-rotate short-tail fairing and a splitter plate as suppressors of vortex-induced vibration," Ocean Eng. **92**, 234–244 (2014).

[27]J. Wu, C. Shu, and N. Zhao, "Numerical investigation of vortex-induced vibration of a circular cylinder with a hinged flat plate," Phys. Fluids **26**, 063601 (2014).

[28]J. Ruiz-Rus, P. Ern, V. Roig, and C. Martínez-Bazán, "Coalescence of bubbles in a high reynolds number confined swarm," J. Fluid Mech. **944**, A13 (2022).

[29]E. Stamhuis and W. Thielicke, "Pivlab–towards user-friendly, affordable and accurate digital particle image velocimetry in matlab," Journal of open research software **2**, 30 (2014).

[30]A. Khalak and C. Williamson, "Motions, forces and mode transitions in vortex-induced vibrations at low mass-damping," J. Fluids Struct. **13**, 813–851 (1999).

[31]C. H. K. Williamson, "Vortex dynamics in the cylinder wake," Annu. Rev. Fluid Mech. **28**, 477–539 (1996).

[32]J. Jiménez-González and F. Huera-Huarte, "Vortex-induced vibrations of a circular cylinder with a pair of control rods of varying size," J. Sound Vib. **431**, 163–176 (2018).

[33]P. Bearman, I. Gartshore, D. Maull, and G. Parkinson, "Experiments on flow-induced vibration of a square-section cylinder," J. Fluids Struct. **1**, 19–34 (1987).

[34]T. K. Prasanth and S. Mittal, "Vortex-induced vibrations of a circular cylinder at low reynolds numbers," J. Fluid Mech. **594**, 463–491 (2008).

Accepted to Phys. Fluids 10.1063/5.0184410

[35]J. Jiménez-González, C. García-Baena, J. Aceituno, and C. Martínez-Bazán, "Flow-induced vibrations of a hinged cavity at the rear of a blunt-based body subject to laminar flow," J. Sound Vib. **495**, 115899 (2021).

View publication stats